Rock Physics-Based Data Assimilation of Integrated Continuous Active-Source Seismic and Pressure Monitoring Data during Geological Carbon Storage

Shams Joon[1]*, Ismael Dawuda[1], Eugene Morgan[1], and Sanjay Srinivasan[1]

[1]The Pennsylvania State University

Summary

There has been substantial controversy concerning the role of geological carbon storage (GCS) in sequestering anthropogenic carbon emissions to mitigate climate change and global warming. Arguments center on the inability to monitor a geological storage site precisely and continuously, especially highlighting the associated costs and spatiotemporal trade-offs when using conventional subsurface monitoring techniques (well logs, core samples, chemical tracers, and 4D seismics). Active surveillance of GCS sites is essential for managing and mitigating potential leaks but is also required by regulation. With the goal of enhancing the monitoring capability at GCS sites, we present a rock physics-based joint data assimilation model to study a popular GCS site at Cranfield, Mississippi, USA. Synthetic continuous active-source seismic monitoring (CASSM) data (in the form of Vp and Qp measurements) and wellbore pressure monitoring data are assimilated with an ensemble of reservoir realizations to monitor gas saturation and reservoir pressure changes over a period of 100 years. Synthetic seismic attributes are generated using rock physics models (RPMs) and wellbore pressure monitoring data are extracted from the ground truth. Two assimilation methods, ensemble Kalman filter (EnKF) and ensemble Kalman smoother (EnKS), are tested in an observation system simulation experiment (OSSE) environment to assess the prediction accuracy of the individual and composite observation systems. The joint monitoring system achieves more accurate estimates of gas saturation and pressure, across the time span from start of injection to end of forecast, as compared to a single type of monitoring tool and irrespective of data assimilation algorithm choice. These results indicate that jointly assimilated data from two types of sensors (in this case, crosswell seismic and downhole pressure) may lead to a more risk-reducing monitoring design. One would expect that more data, vis-à-vis inclusion of a new sensor type, will improve the accuracy of any GCS monitoring system. However, from a practical standpoint, one important question is whether such a gain in accuracy is worth the additional cost associated with the new sensor. This paper focuses on quantifying the gain in accuracy, such that a practitioner can answer this question.

Introduction

Geological sequestration of anthropogenic carbon emissions has gained rapid attention over the past few decades. This process of injecting CO_2 captured from combustion-related sources, such as electricity generation plants into the subsurface for safe and long-term storage (on the order of 1,000 years) presents an innovative opportunity to address issues of climate change (Benson 2006).

The majority of the assessment models compiled by the UN Intergovernmental Panel on Climate Change (IPCC) suggest portfolios of emission reduction technologies that incorporate large-scale deployment of GCS (Metz et al. 2005; IPCC 2014). The Global CCS Institute status report of 2018 indicates that more than 230 $MtCO_2$ has been successfully injected through GCS. Although these numbers are impressive, they amount to a very small fraction of the 55.6 $GtCO_2$ equivalent global greenhouse gas emissions reported in 2018 (Olivier and Peters 2020). The acceptance of GCS is limited by its potential risks and lack of monitoring systems with high enough spatiotemporal resolutions. The primary risks associated with GCS include vertical migration of CO_2 into nearby viable aquifers or the surface, fluid-driven activation of preexisting faults/fractures (human-induced seismicity), and structural damage to nearby producing horizons. This makes the monitoring, verification, and accounting of injected CO_2 crucial to any GCS site. Monitoring, verification, and accounting plans help validate the safe and long-term storage of CO_2, study different efficient storage processes, and assess effective remediation strategies in case of potential leaks (Ramakrishnan et al. 2015).

Data assimilation methods, namely those of the ensemble-based variety, have proven successful at generating probabilistic forecasts from monitoring data. Such methods have been previously adopted to study GCS-related projects (González-Nicolás et al. 2015; Ma et al. 2019; Chen et al. 2020) and are frequently applied in reservoir engineering (Emerick and Reynolds 2013a, 2013b; Evensen et al. 2007; Aanonsen et al. 2009; Raghu et al. 2018) for history-matching purposes. The main attraction of using data assimilation in these contexts lies in its ability to combine the known physics of reservoir systems with observed monitoring data. Ensemble data assimilation methods are based on a Monte Carlo approach that is straightforward to implement and can be easily coupled with multiple observation sources and commercial reservoir simulators. Machine learning models have also made significant advances in the geophysical realm; however, they are often treated as a black box and their purely data-driven nature limits their ability to be applied to reservoir characterization problems beyond pattern recognition (Zhang et al. 2020).

Previous data assimilation applications to reservoir exploration or monitoring problems have primarily focused on one type of sensor data at a time. This is because one form of reservoir data is not directly comparable with another. Previous studies have shown how wellbore pressure gauges can be used to detect potential leaks (Sun and Nicot 2012; Sun et al. 2015); however, locating the source of leak solely from pressure monitoring data is very challenging. This is because, while highly temporal, wellbore pressure sensors only measure pressure at the wellbore. Similarly, while conventional time-lapse seismic surveys provide large spatial resolution, they are limited to discrete time periods that vary from a few months to several years and are expensive. Studies that incorporate multiple observations that

*Corresponding author; email: svj5235@psu.edu

Original SPE manuscript received for review 3 August 2021. Revised manuscript received for review 24 November 2021. Paper (SPE 209585) peer approved 29 December 2021.

include seismic data rely on comparing synthetic seismic amplitudes (generated from forward modeling) with captured seismic amplitudes using petro-elastic models (Huang et al. 1997; Leeuwenburgh et al. 2011; Luo et al. 2016). Another approach is to use seismic and petro-elastic inversion models of captured seismics and compare the inversion results with flow simulation prediction estimates (Abadpour et al. 2013; Ketineni et al. 2020). These methods require reliable petro-elastic models and are sensitive to large model uncertainties. One robust approach to honor both the reservoir simulations and observation data, while accounting for model and observation uncertainty, is through an intermediate assimilation step. This requires the inversion of captured seismic data into elastic properties and comparing them with those estimated through forward modeling (Waggoner et al. 2002; Skjervheim et al. 2007; Fahimuddin et al. 2010; Emerick 2016). Previous studies that have incorporated seismic and production data to estimate reservoir parameters have focused on traditional seismic surveys. The limited temporal resolution and repeatability issues with traditional time-lapse seismic surveys form a bottleneck for improving reservoir characterization estimates. CASSM conducts high-temporal resolution crosswell seismic surveys with excellent repeatability, due to permanent downhole sensor placement.

The use of crosswell CASSM has been successfully implemented at small-scale pilot studies, such as the Frio-II brine pilot to study GCS (Daley et al. 2007). Petrophysical models based on patchy saturation have been successfully implemented to infer the relationship between CO_2 saturation and changes in seismic velocity (Daley et al. 2008, Daley et al. 2011). Additionally, spatiotemporal changes in seismic attenuation as inferred from CASSM data have also been shown to help further constraining CO_2 saturation estimates (Zhu et al. 2017). Our research builds on the successful implementation of these previous studies and uses rock physics-based data assimilation to quantify the impact of combining multiple observations to detect subsurface changes at a GCS facility, such as the Cranfield site in Mississippi, USA. The implications of this study are twofold. First, by taking a stochastic assimilation approach, we can model for noisy measurements and imprecise numerical reservoir models. Second, the use of RPMs to integrate crosswell CASSM and wellbore pressure monitoring data has not been previously studied. In particular, we combine wellbore pressure (p_{wf}) from injection data and seismic attributes such as P-wave seismic velocity (V_p) and attenuation (Q_p) from crosswell seismics. We measure the individual performance of each observation source as well as their combined accuracy during data assimilation. We use EnKF and EnKS assimilation models for this study. The predictive accuracy is measured in the form of assimilation error which is computed by comparing assimilated gas saturation and reservoir pressure with a known ground truth.

The next section provides a detailed background on EnKF and EnKS data assimilation methods followed by the Cranfield model setup. The Results and Discussion section elaborates on the performance of the five observation setups: (1) V_p, (2) Q_p, (3) p_{wf}, (4) V_p and Q_p, and (5) V_p, Q_p, and p_{wf}.

Methods: Data Assimilation of Crosswell CASSM and Wellbore Pressure Data

Reservoir models are built around our uncertain understanding of the subsurface rock and fluid properties. The forecast-predictive accuracy of these models deteriorates as the uncertainty in these properties increases. Measurement error during data acquisition (observation noise), spatiotemporal resolution trade-offs of monitoring systems, and computational costs also limit our ability to accurately model reservoir dynamics. To reduce the uncertainty of model parameters, reservoir models are conditioned to available geophysical measurements via history matching using local and global optimization techniques as well as sampling methods. Data assimilation techniques, such as EnKF and EnKS, aim to combine observation data with numerical models to estimate the state of the system. [See, e.g., Aanonsen et al. (2009) and Cohn (1997) for a more in-depth review of Kalman filter and data assimilation.]

Ensemble-based Kalman filters are reduced-order approaches that avoid storage of the full covariance matrices in memory by estimating model uncertainty in the ensemble space. Ensemble-based data assimilation methods have reduced computational complexity as compared to the original Kalman filter as it propagates high-dimensional systems using a small number of ensemble state realizations. EnKF and EnKS are some of the popular extensions of the Kalman filter (Evensen and Van Leeuwen 2000; Geir et al. 2003; Naevdal et al. 2005; Skjervheim et al. 2011; Raghu et al. 2018). These ensemble methods use the first- and second-order moments of the distribution, and assimilation takes place sequentially in time making it ideal for uncertainty analysis. These ensemble variants present a derivative-free alternative to update state variables by replacing the computationally demanding state covariance matrix of large data sets with sample covariance computed from an ensemble of reservoir realizations. The next section elaborates on the methodology of the two ensemble-based methods in the context of the proposed joint assimilation framework.

Ensemble Kalman Filter. EnKF is a Monte Carlo-based, derivative-free approach of the traditional Kalman filter and was proposed by Evensen to provide a better alternative to the computationally expensive error covariance matrix used in traditional Kalman filter applications (Evensen 1994). The EnKF is an ideal approach to integrate continuous reservoir monitoring data as it leads to, by its nature, a closed-loop reservoir management model that updates as new measurements are made available.

When using EnKF, measurements are assimilated sequentially in time to update the model state variables. The model state propagation (forecast step), sequential measurement, and measurement error statistics are described as

$$X_t = f(X_{t-1}, \alpha), \tag{1}$$

$$Y_t = g(X_t) + \epsilon_t, \tag{2}$$

$$\epsilon_t \sim N(0, \sigma_o^2), \tag{3}$$

where model state X, at time t, is propagated forward in time by a nonlinear function f (numerical simulator) using the static reservoir parameters α (reservoir permeability and porosity) as inputs to generate an ensemble of model state forecasts. In Eq. 1, new measurements are not considered during the forecasts step. The nonlinear function f is a reservoir simulator that forecasts saturation and pressure changes from the previous timestep to the present. The function g maps the state variables from state space to observation space using an RPM. New observations are stored in the observation matrix, denoted by Y_t, and the corresponding error statistics in the form of measurement error is described by a normal distribution with zero mean and covariance σ_o^2.

If we consider gas saturation and reservoir pressure as the variables that describe the dynamic model state, then the background ensemble state variable matrix X_b or the best-guess state estimate, X_{t-1}^a, from the previous assimilation cycle can be represented in the state variable matrix, such that,

$$\mathrm{X}_{t-1}^a = X_t^b = \begin{pmatrix} S_g^1(x, t-1) \ldots S_g^N(x, t-1) \\ P^1(x, t-1) \ldots P^N(x, t-1) \end{pmatrix}, \tag{4}$$

where N represents the number of ensemble members. The gas saturation and reservoir pressure analysis from the previous assimilation cycle are forecasted to the present timestep using a reservoir simulator to generate an updated set of ensemble forecasts, such that,

$$X_t^f = f(X_{t-1}^a, \alpha). \tag{5}$$

Each ensemble member is populated with perturbed realizations of the true α parameters and are used as inputs for simulating the ensembles forward in time using a numerical reservoir simulator denoted by $f()$. Each ensemble, thus, produces distinct forecasts which promote a wide ensemble spread of forecast realizations. Static parameters are assumed to be constant over time; however, they can be augmented to the state variable to update both model state and parameters. Using these forecast ensembles, the ensemble forecast covariance matrix, $C_t^f(x_1, x_2, t)$, is then calculated as:

$$C_t^f(x_1, x_2, t) = \frac{X^f(x_1,t)X^f(x_2,t)^T}{N-1}, \tag{6}$$

where forecast ensemble error $X_t^{f'}$ is defined as:

$$X_t^{f'} = X_t^f - \overline{X}_t^f. \tag{7}$$

The ensemble mean forecast $\overline{X}_t^f$ is a vector with dimensions n, where n is the number of state variables. In this study, the composite observation system consists of continuous seismic attributes (V_p and Q_p) and wellbore pressure monitoring data (p_{wb}) with known error metrics. The observation matrix is represented as:

$$\mathrm{Y}_t^0 = \begin{pmatrix} V_p^1(x,t) \ldots V_p^N(x,t) \\ Q_p^1(x,t) \ldots Q_p^N(x,t) \\ p_{wf}^1(t) \ldots p_{wf}^N(t) \end{pmatrix}. \tag{8}$$

The seismic observations are available along the crosswell section while pressure monitoring data are available at the wellbore as a point measurement. Seismic observations are generated by forward modeling the ground truth gas saturation and pressure. Measurement error in the form of additive Gaussian noise is used to emulate imperfect observations, such that,

$$Y_t^o = g(X_t^{\text{truth}}) + \epsilon_t^o, \tag{9}$$

where measurement error, ϵ_t^o, is a column vector, such that,

$$\epsilon_t^o = (\epsilon_i^1, \epsilon_i^2, \cdots, \epsilon_i^N) \tag{10}$$

The measurement error covariance matrix, C_t^o, can then be computed as:

$$C_t^o = \frac{\epsilon_t^o \epsilon_t^{oT}}{N-1}. \tag{11}$$

The analysis state X^a, at a time t, represents the adjusted forecast state and is computed during the update step, such that,

$$X_t^a = X_t^f + K_t(Y_t^o - HX_t^f). \tag{12}$$

The Kalman gain, K, is the tuning parameter that scales the magnitude of the innovation factor $\left(Y_t^o - HX_t^f\right)$. It is computed as,

$$K_t = C_t^f H^T (HC_t^f H^T + C_t^o)^{-1}, \tag{13}$$

where the H-operator is the measurement matrix that maps state variables to observation space. The H-operator matrix consists of only zero and one element entries in the case of direct measurements (both observations and state variables are comparable). In the case of indirect measurement, such as mapping gas saturation changes from seismic observations, the H-operator matrix is augmented with a nonlinear function. The product of $HX^f(t)$ maps the state vector ensemble forecasts to their corresponding seismic responses in the observation space to compute the innovation factor. One such nonlinear function, in the form of a RPM, is discussed later.

Ensemble Kalman Smoother. The formulation of the EnKS method is like that of EnKF. Both approaches update the state variables sequentially in time, but the EnKS is extended to assimilate in the space-time domain using short time intervals. Unlike the filter approach, the smoother accounts for the space- and time- dependencies by assimilating all observations available in a time window. This is achieved by appending the state variable matrix with state variables from more than one timestep. Like the filter approach, the EnKS then uses the state variable analysis from the last timestep to generate state forecasts but for multiple timesteps. Both the filter and smoother approach provide the exact result in a linear Gaussian case since the smoother is just the filter but for all state variables in a time interval $X_{0:t}$.

In the EnKS formulation, the composite state variable matrix X from time t_0 to t_k is represented as:

$$\tilde{X}_{t_0:t_k}^f = \begin{pmatrix} X^f(x,t_0) \\ \vdots \\ X^f(x,t_k) \end{pmatrix}. \tag{14}$$

The forecast error covariance matrix for the smoother is computed as:

$$\tilde{C}^{f}_{t_o:t_k} = \frac{\tilde{X}^{f}_{t_o:t_k}\tilde{X}'^{T}_{t_o:t_k}}{N-1}. \tag{15}$$

During the EnKS assimilation step, the assimilated state variable ensemble, $\tilde{X}^{a}_{t_o:t_k}$, is formulated as:

$$\tilde{X}^{a}_{t_o:t_k} = \tilde{X}^{f}_{t_o:t_k} + \tilde{C}^{f}_{t_o:t_k}\tilde{H}^{T}\left(\tilde{H}\tilde{C}^{f}_{t_o:t_k}\tilde{H}^{T} + \tilde{C}^{o}_{t_o:t_k}\right)^{-1}\left(\tilde{Y}^{o}_{t_o:t_k} - \tilde{H}\tilde{X}^{f}_{t_o:t_k}\right), \tag{16}$$

where

$$\tilde{Y}^{o}_{t_o:t_k} = \begin{pmatrix} Y_1 \\ \vdots \\ Y_k \end{pmatrix} \tilde{H} = \begin{pmatrix} H_1 \\ \vdots \\ H_k \end{pmatrix}, \tag{17}$$

and the observation error covariance matrix,

$$\tilde{C}^{o}_{t_o:t_k} = \frac{\tilde{\varepsilon}^{o'}_{t_o:t_k}\tilde{\varepsilon}^{o'T}_{t_o:t_k}}{N-1}. \tag{18}$$

The EnKS is a hybrid formulation of a traditional EnKF and ensemble smoother. The EnKS method is sequential in time, but the assimilation cycle incorporates multiple temporal observation from t_{k-1} and t_k. This sequential moving time window helps stabilize the ensemble realizations that are forecasted using the state forecast model. At each data assimilation step, the state variables for all timesteps in the time window are updated and used to guide the state forecast model for the next assimilation cycle.

***H*-Operator.** The innovation proposed in this paper is the embedment of an RPM in the *H*-operator to translate model forecast state variables to their corresponding seismic responses in the observation space. This modification applies to both the EnKF and EnKS algorithms (demonstrated in this paper), and any other Kalman filter-based approach that utilizes the *H*-operator (not shown in this paper). As we estimate the state covariance from the sample covariances of the ensemble of reservoir realizations, we avoid the need to compute a computationally expensive adjoint model to project the state space to the observation space. Instead, we use a (nonlinear) RPM as our forward *H*-operator. This projection of the model state to the observation space allows for direct subtraction between the perturbed observations Y^{o}_{t} and the projected model X^{f}_{t} forecasts during analysis step (Eqs. 12 and 16).

In the case where V_p, Q_p and P_{wf} make up our composite observations, the *H*-operator transforms the state variable forecasts, such that,

$$\mathrm{HX}^{f} = \begin{bmatrix} f(X^{f}_{m}(x,t),\alpha^{1}(x,t)) & \cdots & f(X^{f}_{m}(x,t),\alpha^{N}(x,t)) \\ \vdots & \ddots & \vdots \\ X^{1}_{p}(x,t) & \cdots & X^{N}_{p}(x,t) \end{bmatrix}, \tag{19}$$

where the function f represents the RPM, which takes rock and fluid properties as inputs and outputs seismic attributes, such as V_p and Q_p. The subscript m denotes state variable elements that need to be projected into the observation space and the subscript p denotes the elements of the state vector that are directly being observed. The sets defined by m and p may be mutually exclusive, or there may be overlap. The model parameters, α, contain static reservoir parameters (permeability and porosity) to guide the solution of the RPM. To accommodate for the nonlinearity of the RPM-based *H*-operator, a heuristic covariance localization strategy is adopted by performing a Schur product between the above matrix and an empirically defined correlation matrix with a fixed radius of influence. This localization scheme restricts the influence of observations to state variables that are in proximity to the observations.

The choice of RPM depends on the geological context, the rock and fluid properties, operational parameters of the seismic survey, and available seismic attributes. Later on, we discuss one particular RPM that we use for demonstration purposes, but one could use this general framework to use any one of a variety of RPMs. Furthermore, one could use this proposed framework to include multiple candidate RPMs in the data assimilation by pairing each ensemble with a RPM, such that one has $f^{1}(\cdot)\ldots f^{N}(\cdot)$ in Eq. 19 and making sure to include the necessary inputs for all RPMs in X^{f}_{m} and α.

Data: OSSE Setup

An OSSE environment is a form of synthetic analysis that allows us to estimate the potential impact of a new observation setup before it is deployed in the field. This type of study uses computer models to test out different designs of observation systems and compares their relative performances. **Fig. 1** shows the differences between an OSSE and an operational monitoring system. In an OSSE, the ground truth from the nature run is used to estimate the performance of the observation setup while in an operational system the true dynamics are unknown. **Fig. 2** depicts the operational steps of the Cranfield OSSE environment, containing the RPM-embedded data assimilation routine, used in this study. A "nature run" is first simulated using the known, true, model state and reservoir parameters to generate a ground truth in the form of spatiotemporal changes in CO_2 saturation and reservoir pressure. The true model state and parameters are then used to forward model seismic observations for assimilation. Because the data assimilation utilizes seismic attributes (V_p and Q_p), we only need to synthesize these attributes, along with P_{wf}, as our ground truth observations, as opposed to simulating the raw seismic amplitudes from the survey setup and inverting for the attributes, which would have much higher computational cost. To generate an ensemble of reservoir realizations, the true porosity and permeability are perturbed and are used as input parameters for each ensemble member during the forecast step. The ensemble of reservoir forecasts and the forward modeled seismic observations are then assimilated using a data assimilation system of choice to estimate the model state variables at each timestep. The assimilated model state is then used as the initial condition for generating forecasts for the next timestep, and this iterative process is carried out over the duration of the simulated

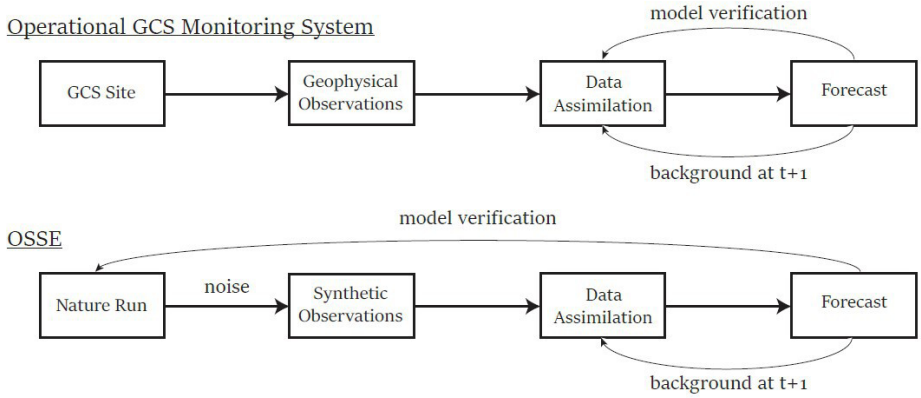

Fig. 1—Model verification approach at an operational GCS site and in an OSSE.

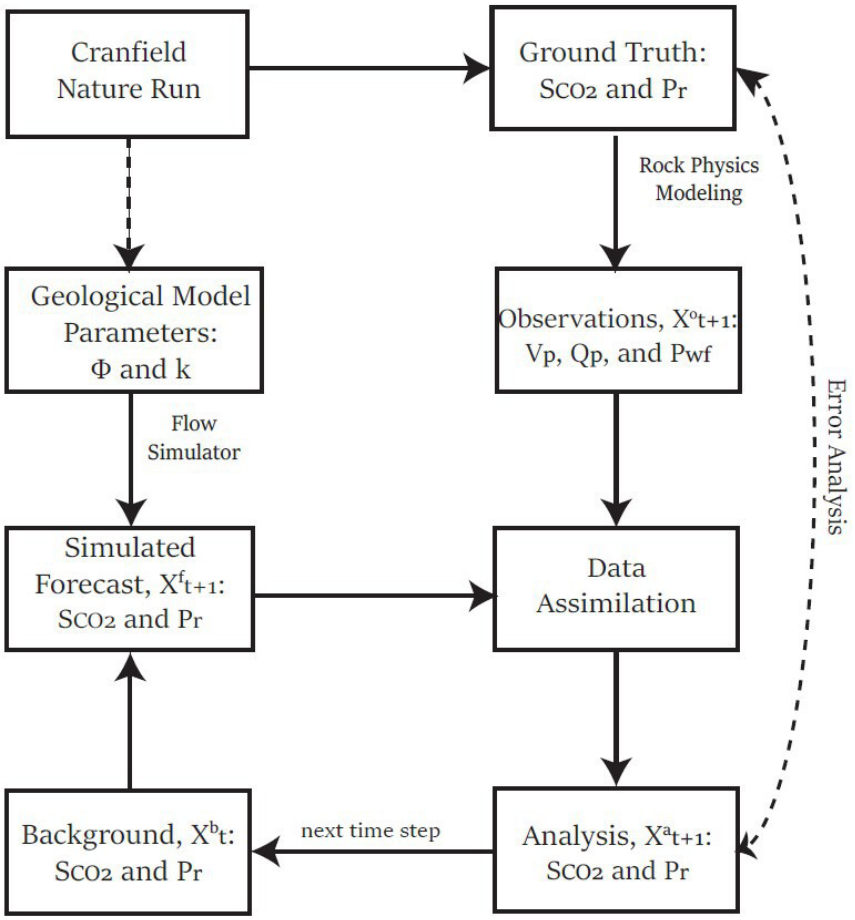

Fig. 2—Proposed crosswell CASSM and pressure monitoring data OSSE environment.

experiment. The predictive accuracy of the monitoring tools and the data assimilation system is estimated by computing the difference between the ground truth and the assimilated state variable estimates. The computational memory requirements scale linearly with the number of ensembles that are used. In the case where the ensemble size is large, the computational bottleneck is the analysis step (Eq. 12 and Eq. 16). The storage requirement of the state variable matrix for EnKF is nN, where n is the state variables and N is the ensemble size. For the EnKS, the storage requirement increases with the number of timesteps that are being assimilated together at each assimilation step. This study uses a relatively small ensemble size, and this reduction comes at a price of a low-rank approximation of the model covariance matrix. Another source of computational cost is during the forecast step where the numerical simulator propagates the ensemble of reservoir realizations forward in time. Both ensemble methods take similar computational time to generate numerical forecasts with EnKS performing slightly slower as it simulates multiple timesteps in one forecast run. The ensemble of reservoir forecasts can be computed in parallel; however, each ensemble takes different amount of time to arrive at a solution and is dependent on the initial conditions, numerical stability, and computational efficiency during the forecast run.

During data assimilation, the model state is estimated and updated by incorporating observations and numerical forecasts. The model state of our system consists of CO_2 saturation and pressure field while model parameters, such as reservoir permeability and porosity, are held constant and are not updated during the assimilation cycle. Instead of assuming the model parameters to be perfectly known, we add a small perturbation to the true model parameters. This allows for testing the assimilation performance under the best of circumstances (very accurate history-matched geomodel) while maintaining a reasonable computational overhead during the data assimilation update step. Significant uncertainty in model parameters can lead to poor state estimates; however, in that case this state estimation approach can be augmented to be a state-parameter estimation problem. In most cases, the uncertainty of reservoir model parameters is addressed by further offline model calibration or by collecting more geophysical data in the form of well logs and coring samples.

One of the added benefits of using an OSSE is that it allows us to synthetically test the risk-based value added of a new observation instrument. In this context of crosswell CASSM and wellbore pressure monitoring data, this implies that we can estimate how each observation attribute (V_p, Q_p, and P_{wf}) improves the state variable (S_g and P_r) estimates in our data assimilation model. To elaborate, we study five scenarios of permanent sensor setups by comparing the predictive accuracy of (1) P_{wf} only, (2) V_p only, (3) Q_p only, (4) V_p and Q_p, and finally (5) V_p, Q_p, and P_{wf}. By comparing these five scenarios, we measure the risk-based value added of different monitoring tools and different combinations of monitoring tools. Intuitively, adding more observation sources should improve our gas saturation and pressure estimates. An error analysis of the different scenarios above will quantify such improvement, which is useful in practice when assessing the value-added contribution of these different sensors. The implementation of these five scenarios affects the dimensionality of the H-operator, the size of the observation matrix, and the computational memory requirement for both data assimilation methods.

Cranfield Model. Cranfield, Mississippi, was identified as a viable site for commercial scale CO_2 injection testing and as of 2003, more than 4 million metric tons of CO_2 has been injected and monitored previously by a team from the Bureau of Economic Geology. We simulate CO_2 injection into the Cranfield reservoir geomodel using a numerical commercial software.

The Cranfield model is a point bar reservoir characterized by two main heterogeneities: lateral and vertical heterogeneities in the form of lateral accretions and heterogeneity introduced by inclined heterolithic stratifications (IHS). The geometry of IHS was modeled with sigmoidal function as described by Thomas et al. (1987), while that of the lateral accretions was modeled with a sine generation function as proposed by Leopold and Langbein (1966). The geometry of the heterogeneities was modeled using a curvilinear grid representative of the point bar geometry. The geologic and geostatistical modeling of the Cranfield reservoir, and the detailed 3D formulation of the gridding procedure are detailed in Dawuda and Srinivasan (2022). **Fig. 3** presents the procedure for the grid generation of the vertical section of the Cranfield reservoir (i.e., the IHS). The same procedure is followed in gridding the lateral accretions. Initially, a domain of interest, which is the region bounded by the reservoir top and bottom surface, is defined as shown in **Fig. 3a**. Grid nodes are then generated along each surface using the length of each surface and the number of gridblocks desired along that surface (see **Fig. 3b**). In **Fig. 3b**, every grid node along a particular gridded surface has a corresponding node on the other gridded surface. Computing the distances between these corresponding pair of nodes and specifying the desired number of gridblocks between the top and bottom surface, grid nodes are subsequently generated between the pairs as illustrated in **Fig. 3c**. The equivalent curvilinear grid is displayed in **Fig. 3d**. In this study, the model contains 10,000 ($20 \times 20 \times 25$ gridblocks).

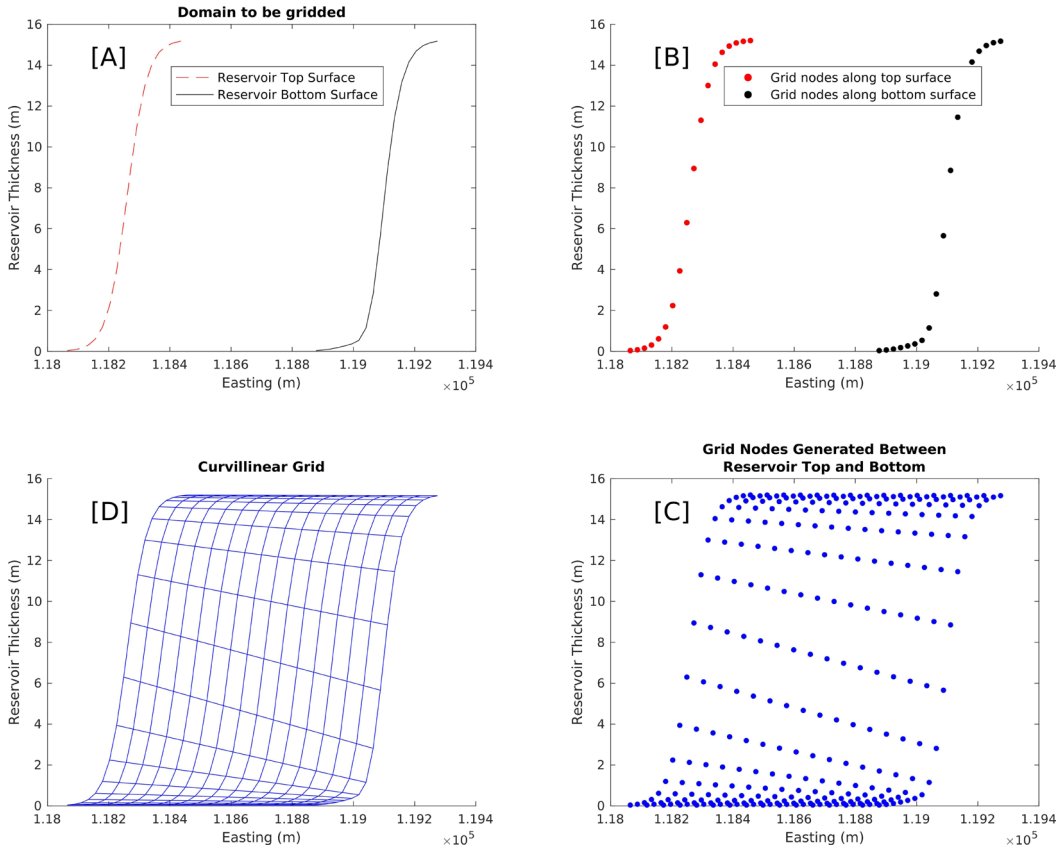

Fig. 3—Curvilinear grid generation procedure: (a) domain to be gridded, (b) gridding along the surfaces, (c) gridding between the two surfaces, and (d) curvilinear grid. Note: The number of gridblocks in a particular direction must be the same for both surfaces.

The reservoir properties (porosity and permeability) were modeled by transforming the curvilinear grid into a rectilinear grid and performing geostatistical interpolation (kriging) on the resulting grid. Wireline logs, from five wells penetrating the point bar reservoir at different locations, gave initial estimates of near-wellbore porosity and permeability, which were then updated through history matching to observed bottomhole pressures, using the curvilinear grid. These values on the curvilinear grid were then transformed to a rectilinear grid for interpolation and then subsequently back-transformed into the original curvilinear grid. **Fig. 4** illustrates the permeability (right) and porosity (left) fields for the Cranfield reservoir model.

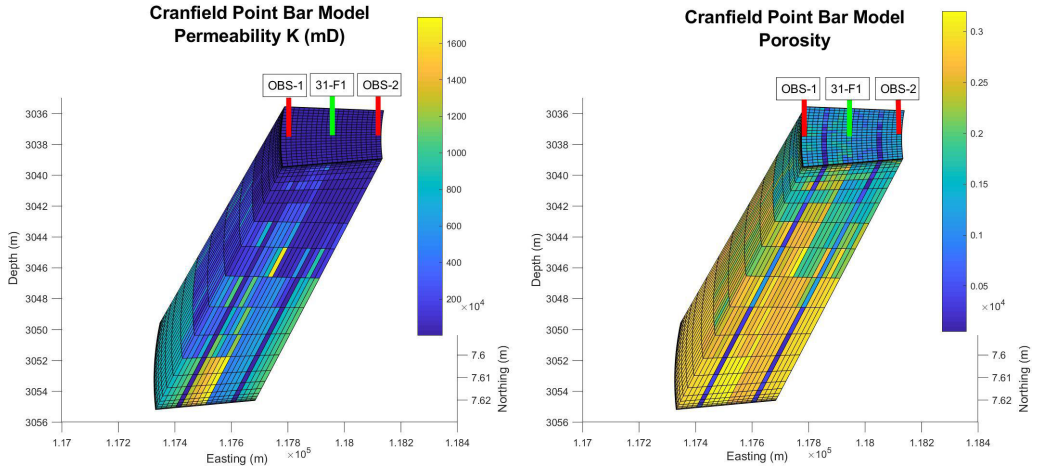

Fig. 4—Ground truth Cranfield reservoir (vertical exaggeration = 45): porosity (left) and vertical permeability (right) in millidarcy.

Permanent Monitoring System Setup

In this section, we discuss the generation of synthetic observation data from our reservoir models. In this paper, we synthesize all observation data from model simulations through the chosen RPM because we wish to evaluate our approach with a known amount of noise in the observations. Furthermore, synthesizing our seismic attribute observations decouples this data assimilation problem from problems associated with estimating seismic attributes, especially regarding seismic attenuation.

Wellbore Pressure. The use of in-situ pressure monitoring gauges to study CO_2 leakage has been proven successful in homogeneous reservoirs but becomes increasingly unreliable in heterogeneous reservoirs where pressure gauges are not able to detect preferential flow channels without significant spatial coverage or prior information about large-scale heterogeneities in the reservoir (Sun and Nicot 2012; Sun et al. 2013). It is difficult to dismiss the value added by pressure monitoring sensors at GCS sites as they provide important information regarding the storage capacity, injectivity, and pressure tolerance of the formation (Simmenes et al. 2013). Furthermore, the EPA guidelines require that the pressure front be tracked over the lifetime of a GCS project, as it is one of the primary factors that drives CO_2 migration (IEA 2010).

For Cranfield GCS OSSE, wellbore pressure monitoring data are generated by adopting additive Gaussian noise to the true pressure field. The wellbore pressure sensor is placed at the injection well (31-F1) at a depth of 3052.7 m as illustrated by **Fig. 4**. The pressure monitoring data are recorded and assimilated every 15 days the first 3 years and then every 6 months for another 97 years. The injection well is shut in after 365 days of CO_2 injection at a constant injection rate of 0.158 m^3/s. Measurement error is assumed to be normally distributed for the ensemble members with a mean of zero and a 5% standard deviation from the true wellbore pressure measurement. The pressure measurement distributions are used to perturb and populate the injection well constrains for each ensemble member. The reservoir is modeled as being in hydrostatic equilibrium and constant pressure boundary conditions are maintained during the nature run and the forecast simulations.

Seismic Attributes. In this study, we generate synthetic V_p and Q_p seismic attributes to emulate the interpreted results from raw crosswell CASSM data. The location of the observation wells (OBS-1 and OBS-2) are shown in **Fig. 4**. A crosswell CASSM survey uses fixed source and receiver sensor locations to continuously monitor seismic waveforms. With the receivers deployed along OBS-1 and OBS-2 and a seismic source at 31-F1, the proposed well placement ensures the CO_2 flowpath is captured along the source-sensor raypath. As injected gas displaces the resident fluid in a reservoir, seismic attenuation and pore pressure around the injection site increases. Several proposed mechanisms explain the sensitivity of seismic attenuation to fluid saturation changes including squirt mechanism (fluid flow between connected pores), direct Biot dissipation, and relative fluid flow across patch boundaries of a multiphase reservoir. In our OSSE system, V_p and Q_p observations are generated by forward modeling the ground truth reservoir simulation using White's patchy gas saturation model as our RPM. In **Fig. 5,** a sample distribution of V_p and Q_p measurements are illustrated along the crosswell geometry. Additionally, the forward operator in the ensemble-based assimilation methods transforms model state forecasts (pressure and gas saturation) from state space to the observation space (seismic attributes and wellbore pressure monitoring data) using the same RPM. In practice, one would estimate these seismic attributes from field seismic data, using conventional methods such as raypath traveltime analysis to determine V_p and spectral ratio method for Q_p.

Rock Physics Model. The use of seismic velocity to infer rock properties is used regularly in the oil and gas industry during exploration. However, the inference obtained from seismic attenuation is underexplored (Carcione et al. 2003). As demonstrated by White (1975), seismic wave velocity and attenuation are affected in the presence of patchy fluid saturation. The size of the gas pocket, permeability and porosity of the reservoir rock, and frequency play a critical role in the seismic responses.

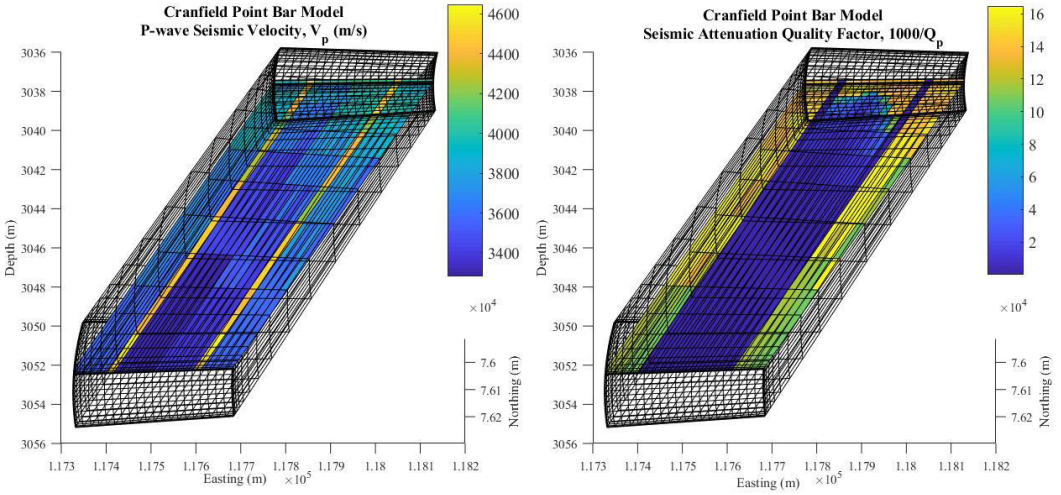

Fig. 5—Forward modeled seismic attributes using White's patchy gas saturation model (vertical exaggeration = 45): V_p (left) in m/s and 1000/Q_p (right). Seismic attributes are measured along the cross-section between the monitoring and injection wells.

White's (1975) model focuses on numerical experiments that aim to demonstrate the effect of patchy gas pockets on the seismic wave propagation. Additionally, extensive laboratory experiments validate this theory and corroborate that seismic attenuation has a strong dependency on fluid saturation (Yin et al. 1992). Although White's model is an idealized representation of partially saturated rock (it only considers concentric spherical pockets of water and gas and ignores interaction between gas pockets), it produces accurate predictions of seismic responses and presents a robust theoretical template that honors Biot's theory of poroelasticity, which predicts the occurrence of a fast and a slow P-wave and the resulting attenuation.

In our experimental design, we use White's model to estimate V_p and Q_p responses when CO_2 is injected into the Cranfield model. White's model considers spherical gas pockets that are located at the center of a cubic array and are saturated with liquid. In particular, two concentric spheres are considered with the outer sphere having the same volume as the cubic array. For each gridblock, we fix the radius of each outer sphere as a function of the gridblock volume. Then, for an outer sphere of radius b and the inner sphere of radius a, we can describe gas saturation as $S_{CO_2} = a^3/b^3$. The patch size has a nontrivial effect on the computed seismic attributes and should be selected based on the sampling frequency during seismic data acquisition using the more-rigorous rederived version of White's model presented by Dutta and Odé (1979a, 1979b) as well as incorporation the corrections pointed out by Dutta and Odé (1979a) regarding the use of P-wave modulus instead of the bulk modulus. During seismic data generation, the Batzle-Wang equations (Batzle and Wang 1992) calculate the density, bulk modulus, and V_p of the water and CO_2 phases, which are then incorporated in White's model to get the V_p and Q_p of the rock and fluid system. The formulation developed by Batzle and Wang does not produce accurate results for CO_2 acoustic properties as they estimate pseudocritical temperatures and pressures using a combination of different natural gases. Xu (2006) presents a modification to the Batzle-Wang equations to estimate acoustic properties of CO_2 by estimating the pseudocritical temperature and pressure corresponding to CO_2 (Xu 2006). Incorporating these modifications to the Batzle-Wang equations, this combined subroutine is called by the forward operator in the update step in data assimilation. We use the Stanford RockPhysics Toolbox in MATLAB® to forward model seismic observations (Mavko et al. 2009). Fluid properties are dynamic and are influenced by reservoir pressure and temperature changes. The subtleties in fluid properties, density, bulk modulus, viscosities, and velocities, become important as CO_2 is injected into the reservoir. We assume a fixed patch size of 0.05 m and a source frequency of 1100 Hz to generate seismic attributes. The elastic modulus of the grain and matrix is estimated by assuming a 90% sandstone and 10% clay mixture with permeability and porosity distribution shown in **Fig. 3** for forward modeling the observed seismic attributes, and perturbed distributions as shown in **Fig. 6** are used as input for the *H*-operator. The fluid properties are estimated by using a reference pressure of 40 MPa and reference temperature of 125°C. The rock and in-situ brine are assumed to be incompressible while the CO_2 compressibility is assumed to be 4.73e−8 Pa^{-1}.

Results

Geophysical observations in the form of V_p, Q_p, and P_{wf} measurements are assimilated at varying time intervals: once every 15 days for the first 3 years and once every 6 months for the subsequent assimilation steps over the 100-year simulation time period. The MATLAB Reservoir Simulation Toolbox is used for numerical reservoir simulations. The reservoir model consists of one injection well that injects CO_2 at a rate of 0.158 m^3/s for a maximum bottomhole pressure of 40 MPa along with two monitoring wells. Wellbore pressure monitoring data are collected only at the injection site.

The ground truth pressure and gas saturation evolution are obtained by running the simulator with the original reservoir model properties. The "true" permeability and porosity values of the ground truth model are shown in **Fig. 4** and the perturbed values are shown in **Fig. 6**. A 5% standard deviation is added to the "true" permeability and porosity fields to generate an ensemble of reservoir static parameters and these perturbed fields are used as input parameters in the numerical simulation portion of the forecast step. The probability distribution of a sample ensemble realization of these perturbed static parameters is shown in **Fig. 6**. An ensemble size of 20 is used and the initial CO_2 saturation is assumed to be 0. The initial reservoir pressure is computed by assuming hydrostatic equilibrium and is equal for all ensemble members. During the assimilation step, the ensemble state is updated to new available measurements and the prediction error is computed by comparing the updated state variables and the ground truth.

The state variable prediction error for the two assimilation methods is plotted in **Fig. 7.** In **Fig. 7**, the prediction error of the EnKF and EnKS methods is plotted for assimilated gas saturation and reservoir pressure in the form of mean bias error (MBE) over the 100 year time duration. The MBE is estimated by summing the difference between the ground truth and the assimilated mean ensemble state variables, of all gridblocks, divided by the total number of gridblocks. In addition to the composite observation system (consisting of V_p, Q_p, and P_{wf}), the uncertainty in prediction estimates of individual observation sources is also presented. Note that both data assimilation

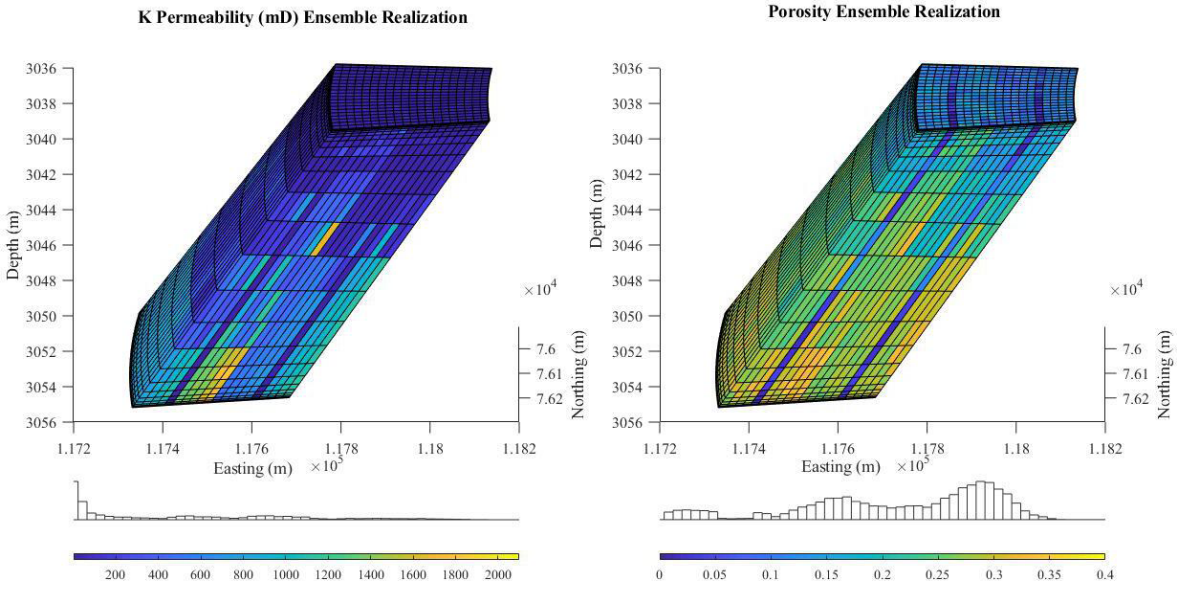

Fig. 6—Perturbed *k*-permeability and porosity distribution used as input parameters for RPM of the *H*-operator (vertical exaggeration = 45). The perturbations follow a normal distribution with a mean of 0 and a standard deviation of 5% from the ground truth.

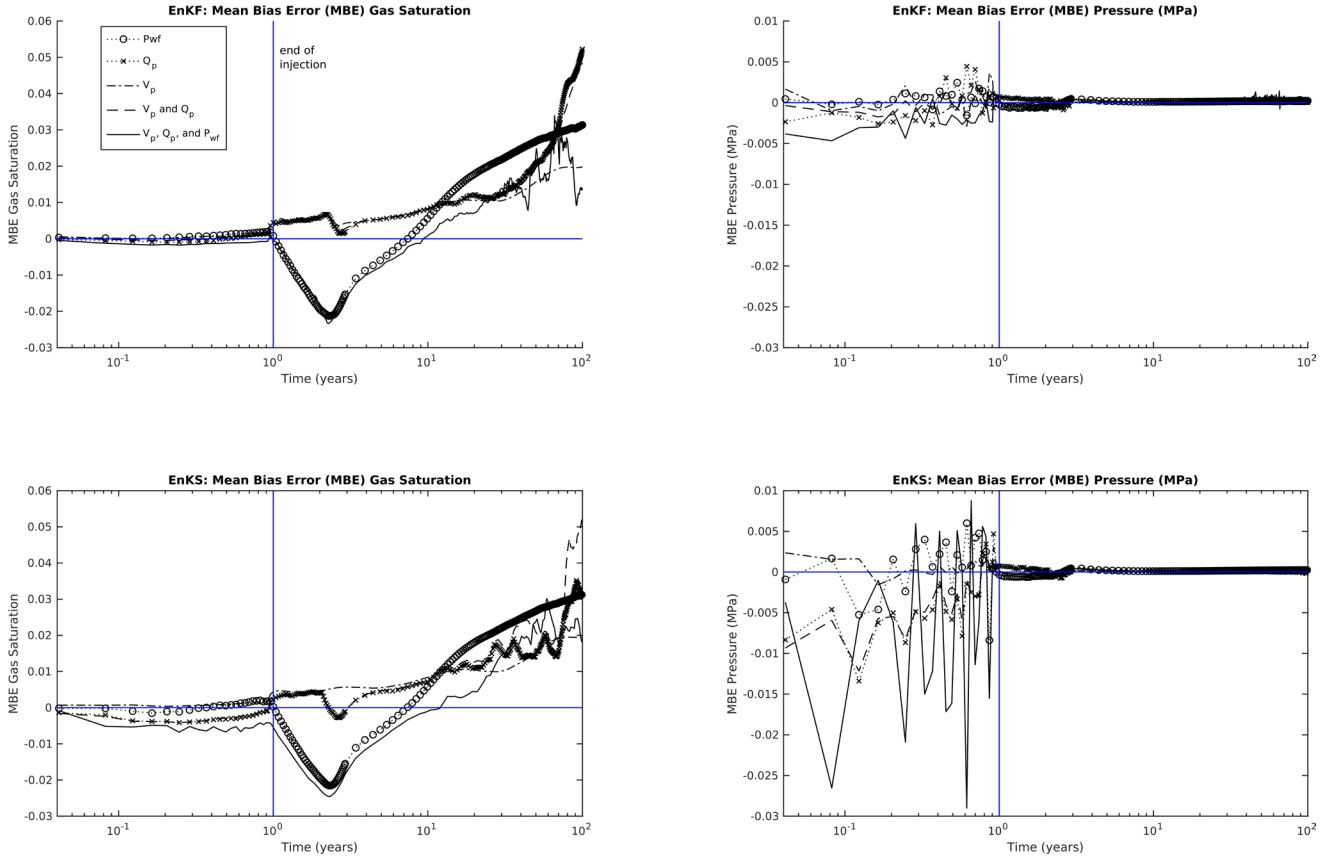

Fig. 7—Gas saturation (left) and reservoir pressure (right) prediction uncertainty using both EnKF (top) and EnKS (bottom) assimilation models. The prediction uncertainty is plotted as the MBE between the ground truth and the assimilated state variables. The black curves represent the time-varying MBE for the EnKF and EnKS assimilated state variables.

method and type of measurement impact the prediction accuracy of the state variable estimates. The state variable prediction error is also computed at different depths of the reservoir along the well. These regions of interests are illustrated by **Fig. 8. Figs. 9 and 10** depicts the gas saturation and gridblock pressure prediction error at these regions for the two assimilation methods. **Fig. 11** depicts the ground truth state of the CO_2 plume at different time intervals (1, 10, 50, and 100 years). **Figs. 12 and 13** depict the CO_2 plume estimates from using the compositive observation system with EnKF and EnKS respectively.

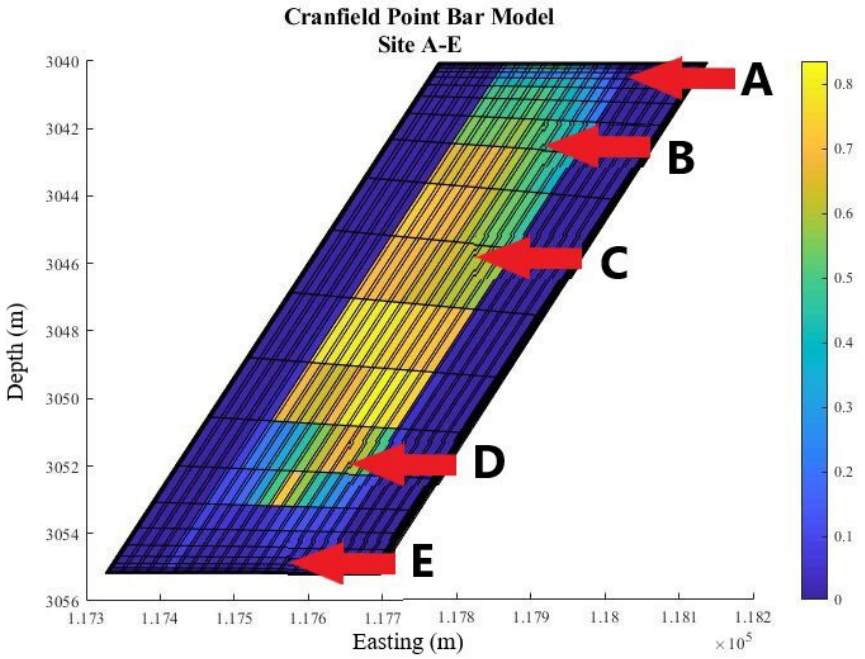

Fig. 8—Cranfield CO_2 saturation profile at the end of the injection period. Site A–E represent multiple points of interest used for spatial uncertainty evaluation.

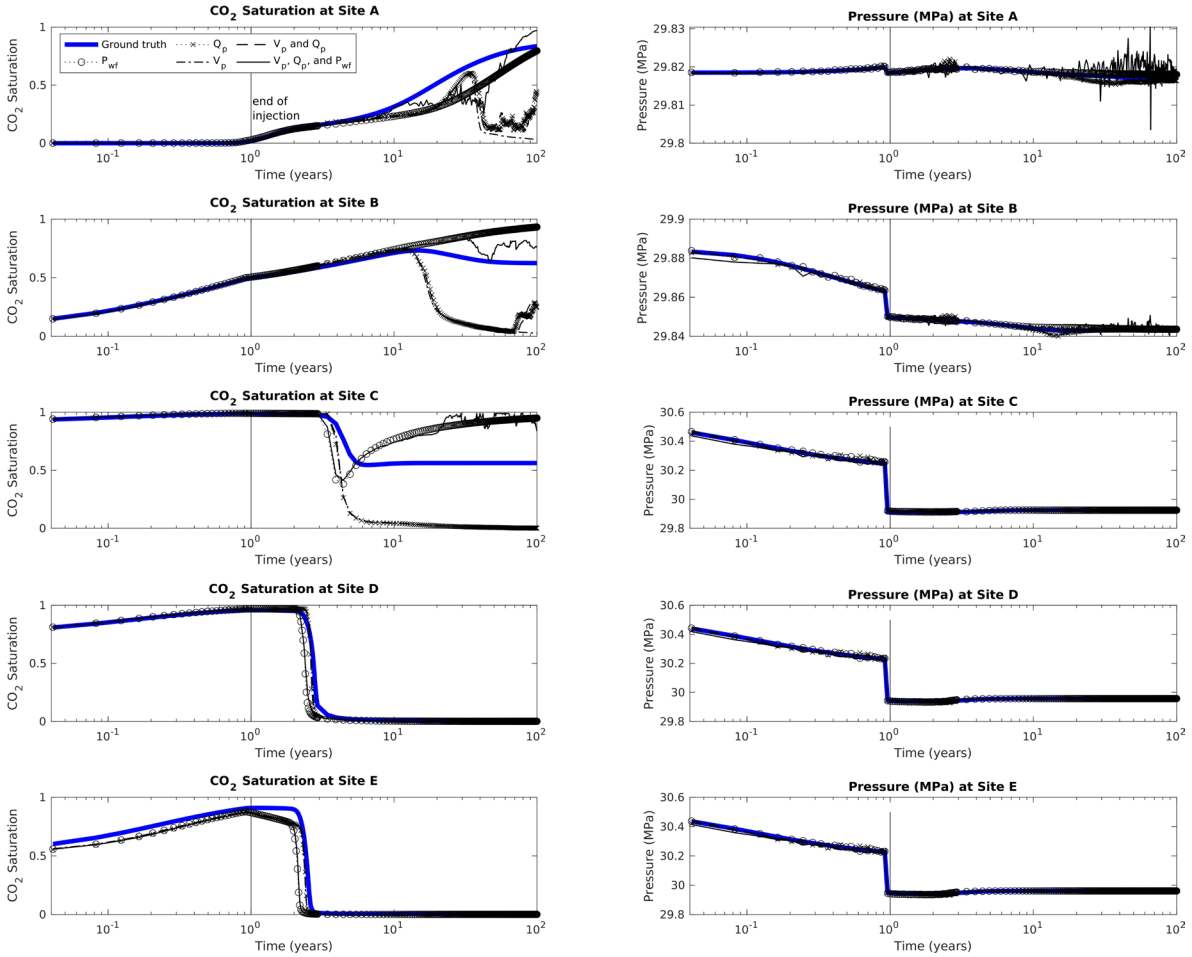

Fig. 9—EnKF CO_2 saturation and reservoir pressure profile (black) plotted against the ground truth (blue).

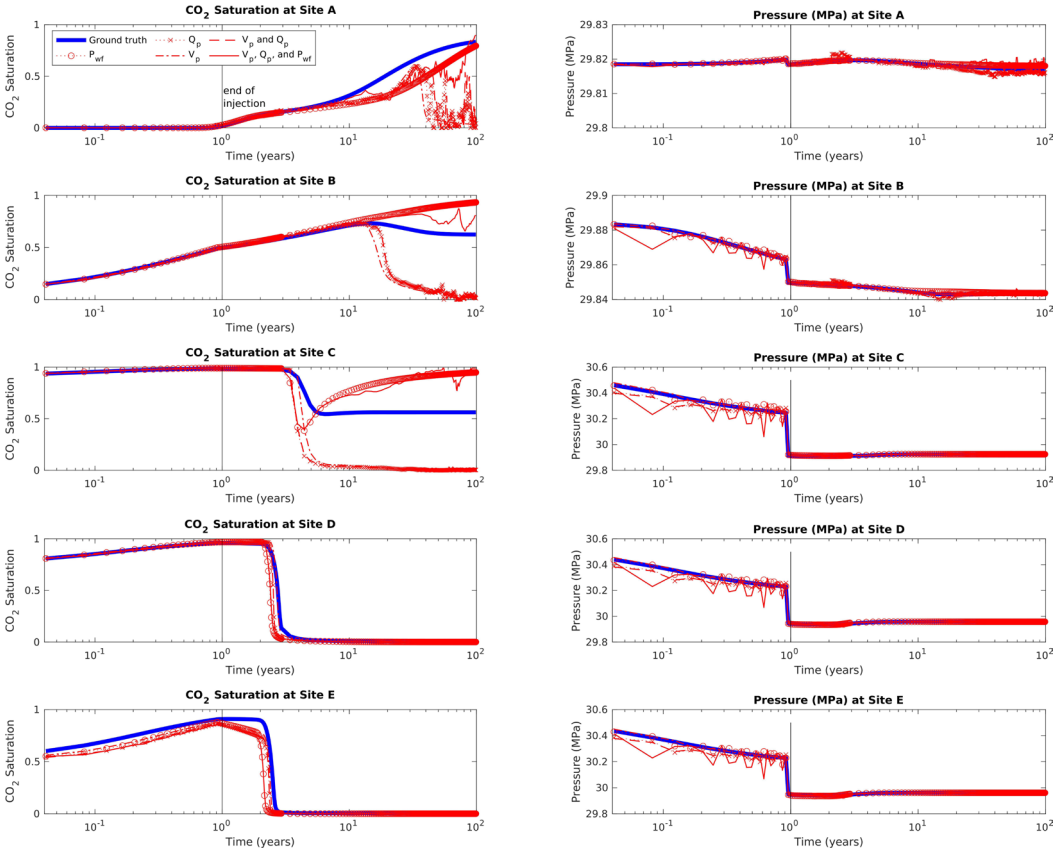

Fig. 10—EnKS CO2 saturation and reservoir pressure profile (red) plotted against the ground truth (blue).

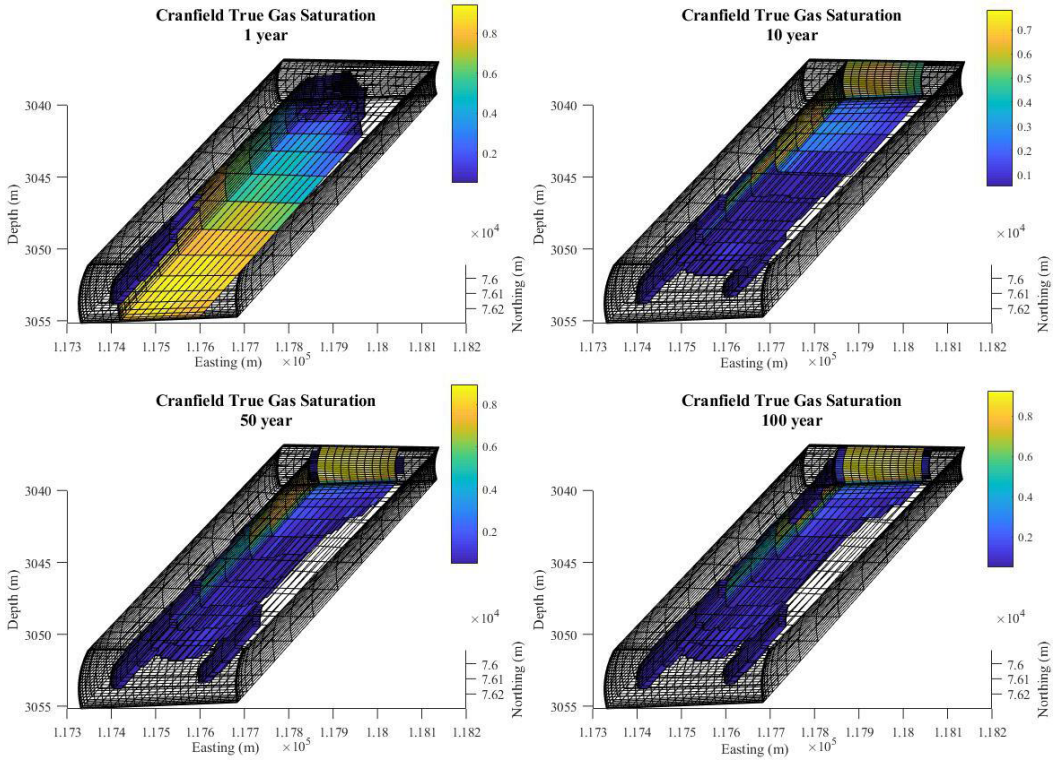

Fig. 11—Ground truth CO_2 plume evolution during the lifetime of the point bar Cranfield reservoir simulation.

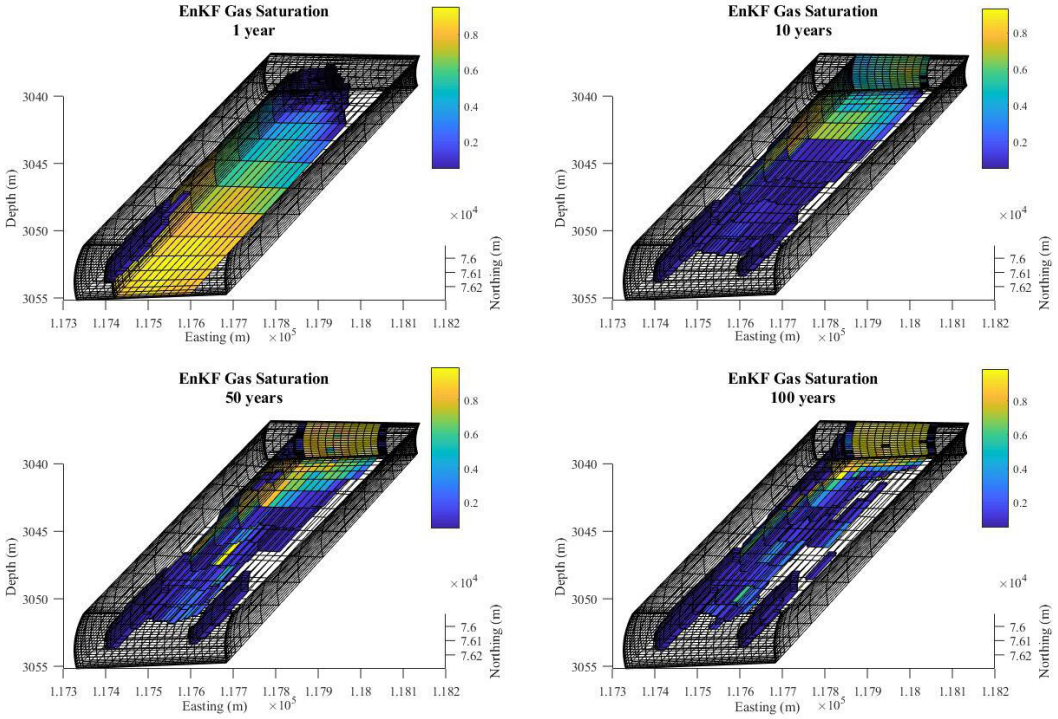

Fig. 12—EnKF-V_p, Q_p, and P_{wf} assimilated CO_2 plume estimates during the lifetime of the point bar Cranfield reservoir simulation.

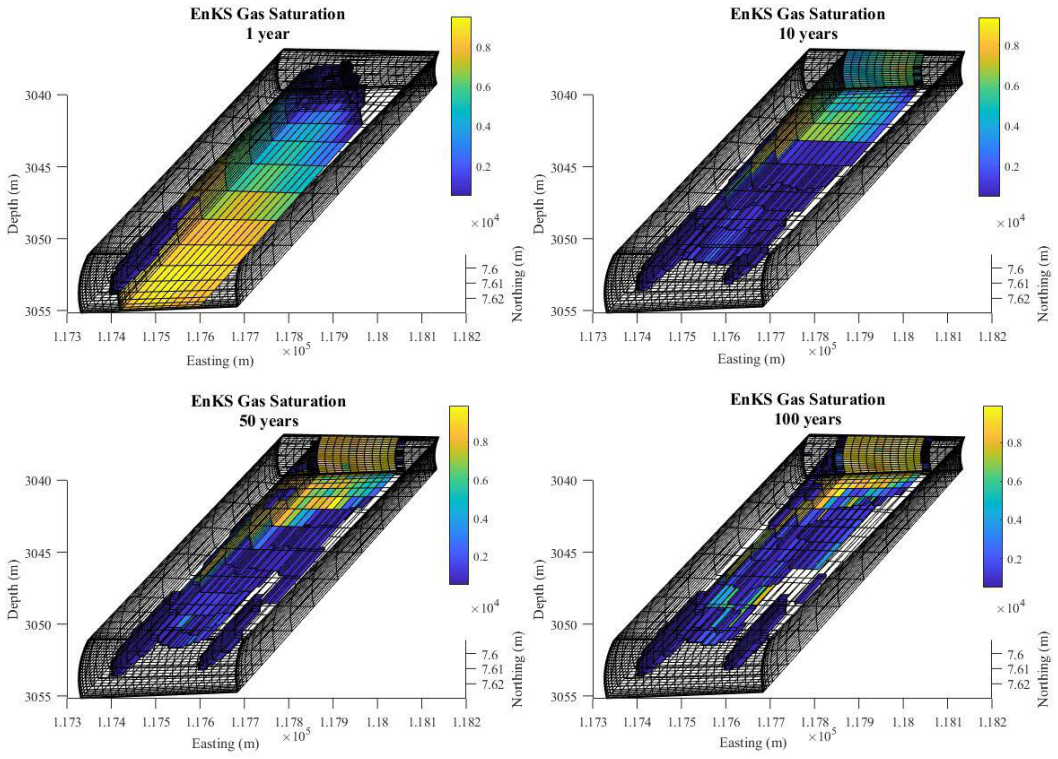

Fig. 13—EnKS-V_p, Q_p, and P_{wf} assimilated CO_2 plume estimates during the lifetime of the point bar Cranfield reservoir simulation.

Discussion

EnKF Experiment. The gas saturation and reservoir prediction error using the EnKF approach are plotted as black curves in the top two plots of **Fig. 7**. All monitoring designs capture the evolution of CO_2 plume during the injection phase with a small amount of prediction error. Assimilated reservoir pressure estimates, however, show the largest uncertainty during the injection phase but stabilize with small prediction uncertainty once the injection well is shut in. During the post-injection phase, the CO_2 saturation prediction accuracy of the monitoring designs decreases over time, and some monitoring designs perform better than others. Among the five EnKF observation

systems, the composite monitoring design (V_p, Q_p, and P_{wf}) and V_p only OSSEs produce the best gas saturation prediction estimates over time. Q_p observations produce large prediction error and over time diverge away from the ground truth. The highly nonlinear nature of assimilating Q_p measurements causes filter divergence in the V_p and Q_p observation system during assimilation as well. The EnKF is vulnerable to over-, under shooting, and filter divergence for highly nonlinear systems. The nonlinear relationship between Q_p and the model state variable, vis-à-vis White's model, demonstrates this vulnerability. Additional parameterization by truncating unreasonable Q_p measurements, increasing the ensemble size, or a different RPM may improve these prediction estimates.

When only P_{wf} measurements are used to update changes in gas saturation and reservoir pressure, the assimilation model heavily relies on the ensemble forecast as the wellbore pressure measurements are point observations. Therefore, we do not observe any significant difference in prediction error between the EnKF-P_{wf} and EnKS-P_{wf} OSSEs. In the case of reservoir models where the reservoir permeability and porosity are generally known, this leads to acceptable assimilated state variable estimates. Increasing the uncertainty of these parameters would cause the simulated forecast to deviate from the true reservoir state over time. We observe similar trends in our EnKF-P_{wf} experiment, where the gas saturation prediction error increases over time due to differences in the permeability and porosity fields of the forecast ensembles and the ground truth. The perturbed permeability fields facilitate flow and transport of CO_2 in regions of low permeability, which leads to increased prediction uncertainty in CO_2 saturation distribution at later stages of the simulation (>10 years).

Combining P_{wf} measurements with seismic attributes improves the prediction accuracy of CO_2 saturation, often outperforming the V_p only monitoring design at later stages of the post-shut-in period. The EnKF is capable of handling different types of measurement data, but using data that are not sensitive to model parameters or do not provide meaningful information negatively impacts the prediction accuracy. In the case of P_{wf} measurement data, Gao et al. (2006) points out that when an injection well reaches its predetermined maximum P_{wf} constraint, the P_{wf} measurement data are no longer useful as it becomes insensitive to the dynamic model parameters. Similar effects are observed during the post-injection period in observation systems that incorporate P_{wf} measurement data. In such a case, removing P_{wf} measurement data from the observation system after the injection well reaches the maximum constraint might be a more suitable approach to explore. The selective use of measurement data, as highlighted by Lee et al. (2016), provides more reliable solutions than assimilating all available data. Wellbore pressure monitoring data can still be incorporated, after shut-in, as a wellbore constraint for numerical simulations during the forecast step.

The ground truth and mean assimilated analysis of CO_2 saturation and pressure at different depths are plotted in **Fig. 9** and their corresponding locations are illustrated in **Fig. 8**. The blue curve represents the ground truth and black curves show the prediction estimates for the different observation system setups. In general, pressure-inclusive monitoring designs perform better at capturing the CO_2 plume movement over the 100-year time period. In particular, the CO_2 saturation levels during the post-shut-in period are captured more accurately than the seismic-only monitoring designs. The seismic-only assimilated CO_2 estimates deviate from the ground truth during the post-shut-in period by underestimating the CO_2 saturation levels at Sites A and B. The composite monitoring design produces CO_2 saturation estimates that most closely resemble the ground truth CO_2 plume evolution. The assimilated pressure prediction estimates of all monitoring designs closely follow the ground truth with small fluctuations observed at Site A near the end of the simulation time period. The hydrostatic equilibrium and constant pressure boundary conditions force the numerical forecasts to follow the true reservoir pressure behavior and thus the pressure predictions do not incur significant prediction error. The increased CO_2 saturation prediction error during the post-shut-in period could be due to reduced post-injection assimilation frequency (from once every 15 days to once every 6 months) which influences the impact observations have on the assimilated analysis and the model error. It contributes to model error by forcing the forecast model (numerical simulator) to evolve the model state, from one step to the next, over a longer duration of time under uncertain reservoir parameters and without the influence of the observations to guide the state evolution forecast. The increased time duration also leads to a narrower forecast ensemble spread due to small differences in initial condition among ensembles and longer forecast durations.

The evolution of CO_2 plume at the end of 1, 10, 50, and 100 years using the V_p, Q_p, and P_{wf} monitoring system are shown in **Fig. 12**. The true CO_2 plume evolution are shown in **Fig. 11**. The maximum uncertainty in CO_2 saturation distribution is located at the boundary of the CO_2 plume which affects the shape and extent of the CO_2 plume.

EnKS Experiment. In the EnKS OSSEs, the same forward-in-time sequential assimilation of observations is carried out. The primary difference between the two assimilation routines is that the EnKS assimilates observations from multiple timesteps during the update step. In the EnKS, three timesteps (45 days during injection, 1.5 years post-shut-in) are assimilated together during each assimilation cycle. This difference leads to more stable prediction estimates for highly nonlinear measurement sources, such as Q_p and to a smaller extent V_p and Q_p, as shown in the bottom two MBE plots of **Fig. 7**. The EnKS assimilation method leads to smaller fluctuations in gas saturation prediction error for Q_p monitoring design; however, increased prediction error is observed in all other monitoring designs. While these prediction errors are not significantly larger than their EnKF counterpart, the EnKS appears to be useful at assimilating highly nonlinear observation sources. For the composite monitoring design, larger fluctuations in pressure predictions are observed during the injection phase with greater negative bias than the EnKF counterpart. The state variable predictions of the P_{wf} only monitoring design for both EnKF and EnKS are unaffected by the choice of data assimilation system.

The assimilated CO_2 saturation and reservoir pressure at different depths of the Cranfield model is plotted in **Fig. 10** against the ground truth. Here, the blue curve represents the ground truth and red curves show the predicted estimates from different observation systems. In both assimilation methods, similar trends in seismic-only monitoring designs are observed at Sites A, B, and C in which the CO_2 saturation levels deviate from the ground truth after 10 years. The composite system produces prediction estimates closest to the ground truth at these sites. Sites D and E are captured accurately for all monitoring designs.

In **Fig. 13**, the evolution of the CO_2 plume as estimated by the EnKS method and V_p, Q_p, and P_{wf} monitoring system is shown at different stages of the GCS experiment: 1 10, 50, and 100 years. These visualizations represent the mean ensemble state of the reservoir when observations and numerical forecasts are optimally combined to monitor model state evolution. The composite observation system produces CO_2 saturation and reservoir pressure estimates that are similar to the ground truth and the EnKF assimilated results.

Conclusions

We have discussed a systematic approach to combine numerical reservoir simulations with crosswell seismic and wellbore pressure data to monitor CO_2 plume movement and pressure changes at an active GCS site in Cranfield, Mississippi. This approach uses a novel rock physics-based data assimilation method and is tested on different types of observation systems consisting of continuous V_p, Q_p, and P_{wf} measurement data. This study shows the impact of multiple observation sources on the prediction uncertainty of gas saturation and pressure estimates. In general, adding more observations yields improved prediction accuracy. In the context of GCS, this means that

combining pressure data with crosswell seismics improves the predictive accuracy of the assimilation model when determining the fate of the injected CO_2. We observe that V_p and Q_p are both sensitive to changes in CO_2 saturation levels but can lead to increased prediction error post-injection because of the underlying RPM. In particular, Q_p is more sensitive than V_p and is challenging to assimilate with a limited ensemble size. The additional local pressure changes near the injection site, in the form of wellbore pressure data improves the prediction estimates at different stages of the GCS project. During injection P_{wf} measurements reduce the gas saturation and pressure prediction error by constraining the CO_2 flow rate from the surface into the reservoir. During post-injection, the reservoir pressure does not change significantly and the P_{wf} measurements avoid overestimation of reservoir pressure. The effect of model error propagation is observed in both assimilation methods in the form of filter divergence. This behavior is more prominent when only one type of observation is assimilated to update the reservoir state. Additionally, the choice of data assimilation method also influences the prediction accuracy, but the differences observed were not significant. The larger point to be made here is that the improvements afforded by different sensors, in this multiphysics fashion, are sensitive to assimilation algorithm choice, and more advanced assimilation algorithms may improve accuracy and show different trade-offs in uncertainty reduction from different sensor combinations. Once the injection well is shut-in, the pressure error in both methods is similar. This workflow is feasible to implement at an active GCS site and presents a closed-loop reservoir management approach to continuously update reservoir properties and parameters as more measurements are made available.

Acknowledgments

Funding for this project is provided by the U.S. Department of Energy's (DOE) National Energy Technology Laboratory (NETL) under award no. DE-FE0031544.

References

Aanonsen, S. I., Nævdal, G., Oliver, D. S. et al. 2009. The Ensemble Kalman Filter in Reservoir Engineering—a Review. *SPE J.* **14** (3): 393–412. SPE-117274-PA. https://doi.org/10.2118/117274-PA.

Abadpour, A., Bergey, P., and Piasecki, R. 2013. 4D Seismic History Matching With Ensemble Kalman Filter - Assimilation on Hausdorff Distance to Saturation Front. Paper presented at the SPE Reservoir Simulation Symposium, The Woodlands, Texas, USA, 18–20 February. SPE-163635-MS. https://doi.org/10.2118/163635-MS.

Batzle, M. and Wang, Z. J. 1992. Seismic Properties of Pore Fluids. *Geophysics* **57** (11): 1396–1408. https://doi.org/10.1190/1.1443207.

Benson, S. M. 2006. Monitoring Carbon Dioxide Sequestration in Deep Geological Formations for Inventory Verification and Carbon Credits. Paper presented at the SPE Annual Technical Conference and Exhibition, San Antonio, Texas, USA, 24–27 September. SPE-102833-MS. https://doi.org/10.2118/102833-MS.

Carcione, J. M., Helle, H. B., and Pham, N. H. 2003. White's Model for Wave Propagation in Partially Saturated Rocks: Comparison with Poroelastic Numerical Experiments. *Geophysics* **68** (4): 1389–1398. https://doi.org/10.1190/1.1598132.

Chen, B., Harp, D. R., Lu, Z. et al. 2020. Reducing Uncertainty in Geologic CO_2 Sequestration Risk Assessment by Assimilating Monitoring Data. *Int J Greenh Gas Control* **94**: 102926. https://doi.org/10.1016/j.ijggc.2019.102926.

Cohn, S. E. 1997. An Introduction to Estimation Theory. *J Meteorol Soc Japan Ser II* **75** (1B): 257–288. https://doi.org/10.2151/jmsj1965.75.1B_257.

Daley, T. M., Ajo-Franklin, J. B., and Doughty, C. 2011. Constraining the Reservoir Model of an Injected CO_2 Plume with Crosswell CASSM at the Frio-II Brine Pilot. *Int J Greenh Gas Control* **5** (4): 1022–1030. https://doi.org/10.1016/j.ijggc.2011.03.002.

Daley, T. M., Ajo-Franklin, J. B., and Doughty, C. 2008. 2008 SEG Annual Meeting. Paper presented at the Integration of Crosswell CASSM (Continuous Active Source Seismic Monitoring) and Flow Modeling for Imaging of a CO2 Plume in a Brine Aquifer, Las Vegas, Nevada, USA, 9–14 November. https://doi.org/10.1190/1.3063941.

Daley, T. M., Solbau, R. D., Ajo-Franklin, J. B. et al. 2007. Continuous Active-Source Seismic Monitoring of C O_2 Injection in a Brine Aquifer. *Geophysics* **72** (5): A57–A61. https://doi.org/10.1190/1.2754716.

Dawuda, I. and Srinivasan, S. 2022. A Hierarchical Stochastic Modeling Approach for Representing Point Bar Geometries and Petrophysical Property Variations (Under Review).

Dutta, N. C. and Odé, H. 1979a. Attenuation and Dispersion of Compressional Waves in Fluid-filled Porous Rocks with Partial Gas Saturation (White Model)—Part I: Biot Theory. *Geophysics* **44** (11): 1777–1788. https://doi.org/10.1190/1.1440938.

Dutta, N. C. and Odé, H. 1979b. Attenuation and Dispersion of Compressional Waves in Fluid-filled Porous Rocks with Partial Gas Saturation (White Model)—Part II: Results. *Geophysics* **44** (11): 1789–1805. https://doi.org/10.1190/1.1440939.

Emerick, A. A. 2016. Analysis of the Performance of Ensemble-Based Assimilation of Production and Seismic Data. *J Pet Sci Eng* **139**: 219–239. https://doi.org/10.1016/j.petrol.2016.01.029.

Emerick, A. A. and Reynolds, A. C. 2013a. Ensemble Smoother with Multiple Data Assimilation. *Comput and Geosci* **55**: 3–15. https://doi.org/10.1016/j.cageo.2012.03.011.

Emerick, A. A. and Reynolds, A. C. 2013b. History-Matching Production and Seismic Data in a Real Field Case Using the Ensemble Smoother With Multiple Data Assimilation. Paper presented at the SPE Reservoir Simulation Symposium, The Woodlands, Texas, USA, 18–20 February. SPE-163675-MS. https://doi.org/10.2118/163675-MS.

Evensen, G. 1994. Sequential Data Assimilation with a Nonlinear Quasi-Geostrophic Model Using Monte Carlo Methods to Forecast Error Statistics. *J Geophys Res* **99** (C5): 10143. https://doi.org/10.1029/94JC00572.

Evensen, G., Hove, J., Meisingset, H. et al. 2007. Using the EnKF for Assisted History Matching of a North Sea Reservoir Model. Paper presented at the SPE Reservoir Simulation Symposium, Houston, Texas, USA, 26–28 February. SPE-106184-MS. https://doi.org/10.2118/106184-MS.

Evensen, G. and van Leeuwen, P. J. 2000. An Ensemble Kalman Smoother for Nonlinear Dynamics. *Mon Wea Rev* **128** (6): 1852–1867. https://doi.org/10.1175/1520-0493(2000)128<1852:AEKSFN>2.0.CO;2.

Fahimuddin, A., Aanonsen, S. I., and Skjervheim, J.-A. 2010. Ensemble Based 4D Seismic History Matching: Integration of Different Levels and Types of Seismic Data. Paper presented at the SPE EUROPEC/EAGE Annual Conference and Exhibition, Barcelona, Spain, 14–17 June. SPE-131453-MS. https://doi.org/10.2118/131453-MS.

Gao, G., Zafari, M., and Reynolds, A. C. 2006. Quantifying Uncertainty for the PUNQ-S3 Problem in a Bayesian Setting With RML and EnKF. *SPE J.* **11** (4): 506–515. SPE-93324-PA. https://doi.org/10.2118/93324-PA.

Geir, N., Johnsen, L. M., Aanonsen, S. I. et al. 2003. Reservoir Monitoring and Continuous Model Updating Using Ensemble Kalman Filter. Paper presented at the SPE Annual Technical Conference and Exhibition, Denver, Colorado, USA, 5–8 October. SPE-84372-MS. https://doi.org/10.2118/84372-MS.

González-Nicolás, A., Baù, D., and Alzraiee, A. 2015. Detection of Potential Leakage Pathways from Geological Carbon Storage by Fluid Pressure Data Assimilation. *Adv Water Resour* **86**: 366–384. https://doi.org/10.1016/j.advwatres.2015.10.006.

Huang, X., Meister, L., and Workman, R. 1997. Reservoir Characterization by Integration of Time-Lapse Seismic and Production Data. Paper presented at the SPE Annual Technical Conference and Exhibition, San Antonio, Texas, USA, 5–8 October. SPE-38695-MS. https://doi.org/10.2118/38695-MS.

IEA. 2010. Federal Requirements Under the Underground Injection Control (UIC) Program for Carbon Dioxide (CO2). In *75 FR 77229*. USA: Environmental Protection Agency.

IPCC. 2014. Climate Change 2014: Mitigation of Climate Change. Contribution of Working Group III to the Fifth Assessment Report of the Intergovernmental Panel on Climate Change. USA.

Ketineni, S. P., Kalla, S., Oppert, S. et al. 2020. Quantitative Integration of 4D Seismic with Reservoir Simulation. *SPE J.* **25** (4): 2055–2066. SPE-191521-PA. https://doi.org/10.2118/191521-PA.

Lee, K., Jung, S., Lee, T. et al. 2016. Use of Clustered Covariance and Selective Measurement Data in Ensemble Smoother for Three-Dimensional Reservoir Characterization. *J Energy Resour Technol* **139** (2). https://doi.org/10.1115/1.4034443.

Leeuwenburgh, O., Brouwer, J., and Trani, M. 2011. Ensemble-Based Conditioning of Reservoir Models to Seismic Data. *Comput Geosci* **15** (2): 359–378. https://doi.org/10.1007/s10596-010-9209-z.

Leopold, L. B. and Langbein, W. B. 1966. River Meanders. *Sci Am* **214** (6): 60–70. https://doi.org/10.1038/scientificamerican0666-60.

Luo, X., Bhakta, T., Jakobsen, M. et al. 2016. An Ensemble 4D Seismic History Matching Framework with Wavelet Multiresolution Analysis - A 3D Benchmark Case Study. Paper presented at the ECMOR XV - 15th European Conference on the Mathematics of Oil Recovery, Amsterdam, Netherlands. https://doi.org/10.3997/2214-4609.201601813.

Ma, W., Jafarpour, B., and Qin, J. 2019. Dynamic Characterization of Geologic CO_2 Storage Aquifers from Monitoring Data with Ensemble Kalman Filter. *Int J Greenh Gas Control* **81**: 199–215. https://doi.org/10.1016/j.ijggc.2018.10.009.

Mavko, G., Mukerji, T., and Dvorkin, J. 2009. *The Rock Physics Handbook: Tools for Seismic Analysis of Porous Media*, second edition. Cambridge, UK: Cambridge University Press. https://doi.org/10.1017/CBO9780511626753.

Metz, B., Davidson, O., H C de, C. et al. 2005. IPCC Special Report on Carbon Dioxide Capture and Storage. Intergovernmental Panel on Climate Change.

Naevdal, G., Johnsen, L. M., Aanonsen, S. I. et al. 2005. Reservoir Monitoring and Continuous Model Updating Using Ensemble Kalman Filter. *SPE J.* **10** (1): 66–74. SPE-84372-PA. https://doi.org/10.2118/84372-PA.

Olivier, J. G. J. and Peters, J. A. H. W. 2020. Trends in Global CO_2 and Total Greenhouse Gas Emissions. PBL Netherlands Environmental Assessment Agency.

Raghu, A., Yang, X., Khare, S. et al. 2018. Reservoir History Matching Using Constrained Ensemble Kalman Filtering. *Can J Chem Eng* **96** (1): 145–159. https://doi.org/10.1002/cjce.22965.

Ramakrishnan, A., Zhang, T. C., and Surampalli, R. Y. 2015. Monitoring, Verification and Accounting of CO_2 Stored in Deep Geological Formations. In *Carbon Capture and Storage*, 159–194. https://doi.org/10.1061/9780784413678.

Simmenes, T., Hansen, O. R., Eiken, O. et al. 2013. Importance of Pressure Management in CO_2 Storage. Paper presented at the Offshore Technology Conference, Houston, Texas, USA, 6–9 May. OTC-23961-MS. https://doi.org/10.4043/23961-MS.

Skjervheim, J.-A., Evensen, G., Aanonsen, S. I. et al. 2007. Incorporating 4D Seismic Data in Reservoir Simulation Models Using Ensemble Kalman Filter. *SPE J.* **12** (3): 282–292. SPE-95789-PA. https://doi.org/10.2118/95789-PA.

Skjervheim, J.-A., Evensen, G., Hove, J. et al. 2011. An Ensemble Smoother for Assisted History Matching. Paper presented at the SPE Reservoir Simulation Symposium, The Woodlands, Texas, USA, 21–23 February. SPE-141929-MS. https://doi.org/10.2118/141929-MS.

Sun, A. Y., Lu, J., and Hovorka, S. 2015. A Harmonic Pulse Testing Method for Leakage Detection in Deep Subsurface Storage Formations. *Water Resour Res* **51** (6): 4263–4281. https://doi.org/10.1002/2014WR016567.

Sun, A. Y. and Nicot, J. P. 2012. Inversion of Pressure Anomaly Data for Detecting Leakage at Geologic Carbon Sequestration Sites. *Adv Water Resour* **44**: 20–29. https://doi.org/10.1016/j.advwatres.2012.04.006.

Sun, A. Y., Nicot, J. P., and Zhang, X. D. 2013. Optimal Design of Pressure-Based, Leakage Detection Monitoring Networks for Geologic Carbon Sequestration Repositories. *Int J Greenh Gas Control* **19**: 251–261. https://doi.org/10.1016/j.ijggc.2013.09.005.

Thomas, R. G., Smith, D. G., Wood, J. M. et al. 1987. Inclined Heterolithic Stratification—Terminology, Description, Interpretation and Significance. *Sediment Geol* **53** (1): 123–179. https://doi.org/10.1016/S0037-0738(87)80006-4.

Waggoner, J. R., Cominelli, A., and Seymour, R. H. 2002. Improved Reservoir Modeling With Time-Lapse Seismic in a Gulf of Mexico Gas Condensate Reservoir. Paper presented at the SPE Annual Technical Conference and Exhibition, San Antonio, Texas, 29 September–2 October. SPE-77514-MS. https://doi.org/10.2118/77514-MS.

White, J. E. 1975. Computed Seismic Speeds and Attenuation in Rocks with Partial Gas Saturation. *Geophysics* **40** (2): 224–232. https://doi.org/10.1190/1.1440520.

Xu, H. 2006. Calculation of CO2 Acoustic Properties Using Batzle-Wang Equations. *Geophysics* **71** (2): F21–F23. https://doi.org/10.1190/1.2187734.

Yin, C.-S., Batzle, M. L., and Smith, B. J. 1992. Effects of Partial Liquid/Gas Saturation on Extensional Wave Attenuation in Berea Sandstone. *Geophys Res Lett* **19** (13): 1399–1402. https://doi.org/10.1029/92GL01159.

Zhang, G., Wang, Z., Mohaghegh, S. et al. 2020. Pattern Visualization and Understanding of Machine Learning Models for Permeability Prediction in Tight Sandstone Reservoirs. *J Pet Sci Eng* **200**: 108142. https://doi.org/10.1016/j.petrol.2020.108142.

Zhu, T., Ajo-Franklin, J. B., and Daley, T. M. 2017. Spatiotemporal Changes of Seismic Attenuation Caused by Injected CO_2 at the Frio-II Pilot Site. *J Geophys Res Solid Earth* **122** (9): 7156–7171. https://doi.org/10.1002/2017JB014164.